Signatures of β−Peptide Unfolding in Two-Dimensional Vibrational Echo Spectroscopy: A Simulation Study

3 AUTHORS, INCLUDING:

Shaul Mukamel

University of California, Irvine

852 PUBLICATIONS   **23,577** CITATIONS

Signatures of β-Peptide Unfolding in Two-Dimensional Vibrational Echo Spectroscopy: A Simulation Study

C. Scheurer,[†] A. Piryatinski,[‡] and S. Mukamel*

Contribution from the Department of Chemistry, University of Rochester, Rochester, New York 14627

Received September 18, 2000. Revised Manuscript Received January 22, 2001

Abstract: An ensemble of exciton Hamiltonians for the amide-I band of the folded and unfolded states of a helical β-heptapeptide is generated using a molecular dynamics (MD) simulation. The correlated fluctuations of its parameters and their signatures in two-dimensional (2D) vibrational echo spectroscopy are computed. This technique uses infrared pulse sequences to provide ultrafast snapshots of molecular structural fluctuations, in analogy with multidimensional NMR. The present study demonstrates that, by combining a method of calculating the vibrational Hamiltonian from MD snapshots and the nonlinear exciton equations (NEE), it may be possible to simulate realistic multidimensional IR spectra of chemically and biologically interesting systems.

I. Introduction

The three-dimensional structure of proteins determines their activity as enzymes, receptors, regulatory factors, and all other functional elements in nature. The folding of peptides and proteins from a random coil into their native three-dimensional structure is therefore a process of fundamental importance in molecular biology. A detailed understanding of protein folding should also greatly facilitate pharmaceutical drug design. Gaining insight into the folding process is a tremendous task due to its complexity and the multitude of time scales on which it occurs, ranging from nanoseconds for loop formation, hydrophobic collapse, or β-sheet formation to microseconds for α-peptides to reach their native fold.[1,2] A number of techniques, including optical and infrared (IR) absorption, fluorescence, NMR spectroscopy,[3−5] small angle X-ray scattering (SAXS),[6,7] and time-resolved Laue diffraction,[8,9] have been used to study the folding process in proteins and peptides. These methods provide either indirect (e.g., NMR relaxation measurements) or time-averaged (due to a nanosecond or longer detection window) information about the structure and potential energy surface of these complex biological systems along the folding path.

The present study focuses on the vibrational $1600-1700$ cm^{-1} amide-I band in proteins which is commonly used to study unfolding processes in temperature jump (T-jump) experiments by ordinary one-dimensional (1D) IR spectroscopy.[2] The band originates from the stretching motion of the CO bond coupled to in-phase N−H bending and C−H stretching. This mode has a strong transition dipole moment and is clearly distinguishable from other vibrational modes of the amino acid residues. An early study of symmetric model peptides[10] demonstrated that the transition dipole coupling between CO stretching modes in different peptide bonds results in a delocalization of the amide-I states. These states can be described by vibrational excitons,[10,11] using the Frenkel exciton model developed originally to treat delocalized electronic[12,13] and vibrational[14−16] excitations in molecular crystals and aggregates. The dependence of the dipole−dipole coupling on the relative orientations and distances of the interacting dipoles yields an amide-I band signature that depends on the three-dimensional structure of the protein. The different secondary structure elements occurring in proteins result in characteristic amide-I signatures which form the basis of polypeptide and protein structure determinations.[17,18]

Good agreement with experimental 1D spectroscopy has been obtained for calculated absorption line shapes of a few mid-size globular proteins with known structures, assuming dipole−dipole coupling between the peptide groups.[11] However, the information content of these highly averaged 1D spectra is comparatively low. The complicated three-dimensional structure of proteins leads to overlapping bands that correspond to the different secondary structural elements. These bands are additionally inhomogeneously broadened by conformational fluctuations of the secondary structure elements and by coupling

---
* Author for correspondence. E-mail: mukamel@chem.rochester.edu.
† E-mail: chris@feynman.chem.rochester.edu.
‡ E-mail: apiryat@feynman.chem.rochester.edu. Present address: Department of Chemistry, University of Wisconsin, Madison, WI 53706.

(1) Karplus, M.; Shakhnovich, E. In *Protein Folding*; Creighton, T. E., Ed.; W. H. Freeman & Co.: New York, 1992; pp 127−195.
(2) Valentine, J. S., Ed. Protein Folding, Special Issue of *Acc. Chem. Res.* **1998**, *31*, 697−780.
(3) Kuhn, T.; Schwalbe, H. *J. Am. Chem. Soc.* **2000**, *122*, 6169.
(4) Balbach, J. *J. Am. Chem. Soc.* **2000**, *122*, 5887.
(5) Pfuhl, M.; Driscoll, P. *Philos. Trans. R. Soc. London, Ser. A* **2000**, *358*, 513.
(6) Segel, D. J.; Bachmann, A.; Hofrichter, J.; Hodgson, K. O.; Doniach, S.; Kiefhaber, T. *J. Mol. Biol.* **1999**, *288*, 489.
(7) Arai, S.; Hirai, M. *Biophys. J.* **1999**, *76*, 2192.
(8) Perman, B.; Anderson, S.; Schmidt, M.; Moffat, K. *Cell. Mol. Biol.* **2000**, *46*, 895.
(9) Hori, T.; Moriyama, H.; Kawaguchi, J.; Hayashi-Iwasaki, Y.; Oshima, T.; Tanaka, N. *Protein Eng.* **2000**, *13*, 527.

(10) Krimm, S.; Bandeker, J. *J. Adv. Protein Chem.* **1986**, *38*, 181.
(11) Torii, H.; Tasumi, M. *J. Chem. Phys.* **1992**, *96*, 3379.
(12) Mukamel, S. *Principles of Nonlinear Optical Spectroscopy*; Oxford University Press: New York, 1995.
(13) Pope, M.; Swenberg, C. E. *Electronic Processes in Organic Crystals and Polymers*; Oxford University Press: New York, 1999.
(14) Bernstein, E. R.; Colson, S. D.; Kopelman, R.; Robinson, G. W. *J. Chem. Phys.* **1968**, *48*, 5596.
(15) LeSar, R.; Kopelman, R. *J. Chem. Phys.* **1977**, *66*, 5035.
(16) LeSar, R.; Kopelman, R. *Chem. Phys.* **1978**, *29*, 289.
(17) Dyer, R. B.; Gai, F.; Woodruff, W. H.; Gilmanshin, R.; Callender, R. H. *Acc. Chem. Res.* **1998**, *31*, 709.
(18) Hamm, P.; Lim, M.; DeGrado, W. F.; Hochrasser, R. M. *Proc. Natl. Acad. Sci. U.S.A.* **1999**, *96*, 2036.

to the local environment due to the solvent, yielding a highly congested amide-I band.

Multiple pulse coherent spectroscopic techniques constitute an effective remedy for this problem.[19−22] Nonlinear-IR and Raman techniques offer a broad range of novel types of multidimensional experiments by varying time delays between pulses, carrier frequencies, phases, and envelopes. Spreading the signal in several dimensions by probing the various time delays increases the resolution and decreases signal overlap, as is widely known from multidimensional NMR.[23,24] Multiple pulse coherent experiments can also selectively eliminate certain line-broadening effects. Furthermore they allow the employment of techniques for background suppression and spectral editing,[25] that is, suppression of neighboring peaks or certain classes of peaks, in analogy with NMR spectroscopy.

The ultrafast nonlinear optical and vibrational spectroscopies additionally provide detection on the femtosecond time scale and have therefore the capacity to directly follow the elementary events in the unfolding process in great detail and with high time resolution.[2,12,19−21,26−29] The multidimensional spectra obtained from these new techniques are snapshot images of the molecular geometry at different stages of the folding process. Yet the structural information is not readily accessible. Similar to NMR or EPR[30] the information that is extracted from the two-dimensional (2D) spectra consists of transition frequencies, couplings, and line shapes that are determined by an effective spectroscopic Hamiltonian. The effective vibrational Hamiltonian is directly related to the motion of the molecule, and its structure is considerably more complex than that of a spin-$\frac{1}{2}$ Hamiltonian. It is therefore important to be able to compute the respective Hamiltonian parameters from first principles, especially for large systems where the spectra become complicated and hard to analyze without microscopic modeling. In this paper we present an approach that combines protein MD simulations with a Hamiltonian parametrized in terms of the peptide geometry to obtain a fluctuating exciton Hamiltonian that explicitly depends on the geometries taken from an MD trajectory.

In resonant multidimensional IR spectroscopies the excitation pulses couple directly to the transition dipoles of the chromophores. The lowest-order techniques which can be used in noncentrosymmetric media consist of three pulses (Figure 7). The two time delays between the three pulses plus the detection time provide three-dimensional snapshot images of molecular structure and its fluctuations. The simulation of the signal requires the calculation of the third-order response function which depends on the complete set of one- and two-exciton states and their coupling to a thermal bath. The dynamics of the one- and two-exciton manifold is most efficiently described using the nonlinear exciton equations (NEE).[31]

We use the NEE to calculate the multidimensional vibrational response of proteins in the amide-I region based on the fluctuating exciton Hamiltonian for the 2D photon echo (vibrational echo) technique, which has been analyzed in detail for small simplified model systems.[20] The use of an ensemble of MD structures provides a microscopic model of the changes in the chromophore transition frequencies and the interchromophore couplings. This goes beyond commonly used simplified uncorrelated Gaussian diagonal and off-diagonal disorder models for inhomogeneous broadening.[20,32] We will demonstrate this by simulating the amide-I band spectroscopic signatures of unfolding for an artificial β-peptide. This peptide was chosen since in a recent theoretical study[33] it was found that a considerable advantage over the naturally occurring α-polypeptides is that in MD simulations the β-peptides fold on a nanosecond time scale. The lower limit for proteins as well as most α-peptides to fold is believed to be microseconds, which is orders of magnitude longer than the typically achievable MD simulation times. The β-peptides therefore constitute very promising model systems to study folding, unfolding, and refolding of polypeptides. NMR experiments yield higher unfolding temperatures than those found in the simulations,[34] and a very recent MD study shows a dependence of the unfolding temperature on the force-field.[35] Ultrafast vibrational spectroscopy has the capability to provide new information and an independent direct view of the unfolding process.

In section II we introduce the β-peptides, discuss some of their properties, and present the MD unfolding simulation of the β-heptapeptide with the chemical structure shown in Figure 1. The vibrational Hamiltonian and a statistical analysis of its parameters are given in section III. The 2D vibrational echo spectra are presented in section IV and we conclude by a general discussion in section V.

II. Molecular Dynamics Simulation of β-Peptides: Folded and Unfolded Structures

Until recently it had been commonly assumed that computer simulation of peptide folding under realistic conditions would not be possible in the forseeable future. This paradigm has been changed by the interesting class of artificial β-peptides,[33] studied and synthesized by Seebach et al.[36] These polypeptides are built from synthetic β-amino acid residues which have an extra backbone carbon compared with the natural α amino acids ($-HN-HC^{\beta}R^3-HC^{\alpha}R^2-CO-$, $R^{2,3}$ being the side chains). They can be synthetically tailored to adopt different secondary structure elements, depending on the side chain composition and position.[37] The large class of secondary structure elements found in β-peptides includes left- and right-handed 3_1 helices with all carbonyl groups pointing either in the same direction

(19) Mukamel, S.; Piryatinski, A.; Chernyak, V. *Acc. Chem. Res.* **1999**, *32,* 145.

(20) Piryatinski, A.; Tretiak, S.; Chernyak, V.; Mukamel, S. *J. Raman Spectrosc.* **2000**, *31,* 125.

(21) Mukamel, S.; *Annu. Rev. Phys. Chem.* **2000**, *51, 691.*

(22) Merchant, K. A.; Thompson, D. E.; Fayer, M. D., submitted 2000.

(23) Cavanagh, J.; Fairbrother, W. J.; Palmer, I.; Arthur G.; Skelton, N. J. *Protein NMR Spectroscopy: Principles and Practice*; Academic Press: San Diego, 1996.

(24) Ernst, R. R.; Bodenhausen, G.; Wokaun, A. *Principles of Nuclear Magnetic Resonance in One and Two Dimensions*; Clarendon Press: Oxford, 1987.

(25) Schoenlein, R.; Mittleman, D.; Shiang, J.; Alivisatos, A.; Shank, C. *Phys. Rev. Lett.* **1993**, *70*, 1014.

(26) Mukamel, S.; Hochstrasser, R., Eds. Special Issue of *Chem. Phys.* **2001**.

(27) Rector, K. D.; Kwok, A. S.; Ferrante, C.; Tokmakoff, A.; Rella, C. W.; Fayer, M. D. *J. Chem. Phys.* **1997**, *106*, 10027.

(28) Okumura, K.; Tokmakoff, A.; Tanimura, Y. *J. Chem. Phys.* **1999**, *111*, 492.

(29) Hamm, P.; Lim, M.; DeGrado, W. F.; Hochstrasser, R. M. *J. Chem. Phys.* **2000**, *112,* 1907.

(30) Freed, J. H. *Annu. Rev. Phys. Chem.* **2000**, *51*, 655.

(31) Chernyak, V.; Zhang, W. M.; Mukamel, S. *J. Chem. Phys.* **1998**, *109, 9587.*

(32) Hamm, P.; Lim, M.; DeGrado, W. F.; Hochstrasser, R. M. *J. Phys. Chem. A* **1999**, *103,* 10049.

(33) Daura, X.; Gademann, K.; Jaun, B.; Seebach, D.; van Gunsteren, W. F.; Mark, A. E. *Angew. Chem., Int. Ed.* **1999**, *38*, 236.

(34) Gademann, K.; Jaun, B.; Seebach, D.; Perozzo, R.; Scapozza, L.; Folkers, G. *Helv. Chim. Acta* **1999**, *82*, 1.

(35) Damm, W.; van Gunsteren, W. F. *J. Comput. Chem.* **2000**, *21*, 774.

(36) Seebach, D.; Abele, S.; Gademann, K.; Guichard, G.; Hintermann, T.; Jaun, B.; Matthews, J.; Schreiber, J. *Helv. Chim. Acta* **1998**, *81*, 932.

(37) Gademann, K.; Hintermann, T.; Schreiber, J. V. *Curr. Med. Chem.* **1999**, *6*, 905.
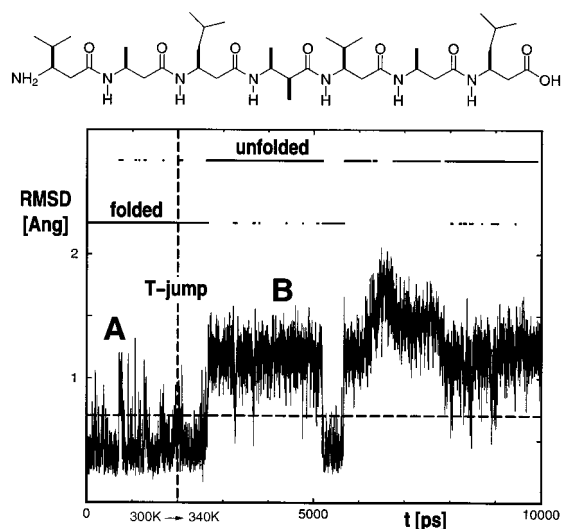
Figure 1. Time-dependent backbone root-mean-square deviation (RMSD) with respect to the NMR solution structure for the β-heptapeptide with the given chemical structure. The T-jump occurs at $t = 2$ ns where the temperature is raised from 300 to 340 K (see text for details).

or with alternating orientation, helices of 3_{14} and 12/10 type, parallel and antiparallel sheet structures, hydrogen-bonded 10-, 12-, and 14-membered rings, and, finally, turn motifs. In contrast to natural α-peptides, the β-petides are resistant against degradation by proteolytic enzymes and have therefore recently attracted much attention as potential peptide mimetics.[37]

The present study focuses on the β-heptapeptide H-β^3-HVal-β^3-HAla-β^3-HLeu-(S,S)-β^3-HAla(αMe)-β^3-HVal-β^3HAla-β^3-HLeu-OH. All side chains of this β-peptide are in position R^3 except for residue number four, which is methylated at both R^2 and R^3 as can be seen from its chemical structure shown in Figure 1. From the unfolding and refolding events observed in a long (50 ns) trajectory of this β-heptapeptide in methanol, Daura et al. inferred that both structures have equal probability at 340 K where the free energy of folding vanishes.[33] The same group recently reported a dependence of the unfolding temperature on the force-field parameters used and concluded that it might be as high as 360 K[35] which is in better agreement with an NMR study.[34]

This system has several additional desirable properties. First, MD simulations with the GROMOS96 force field[38] were in agreement with all available experimental NMR data without the inclusion of artificial constraints. Second, although the β-heptapeptide adopts a well-defined stable fold at 300 K, the system does not represent a trivial folding problem. Each β-amino acid residue has three degrees of freedom for backbone rotation compared to two for an α-amino acid, making the conformational search problem roughly equivalent to that of an α-decapeptide. Third, as the commonly used force fields were not developed for β-amino acids, there can be no suspicion that the force field used might have been artificially adjusted to favor the experimental fold. Finally, methanol is, like water, a strongly hydrogen-bonding solvent. Methanol has, however, a lower density, making it a computationally less expensive solvent in which to simulate folding. For these reasons the heptapeptide in methanol is an ideal system for unfolding studies. It should be noted that the simulated folding time scale is very sensitive

(38) van Gunsteren, W. F.; Billeter, S. R.; Eising, A. A.; Hünenberger, P. H.; Krüger, P.; Mark, A. E.; Scott, W. R. P.; Tironi, I. G. *Biomolecular simulation: The GROMOS96 manual and user guide*; vdf Hochschulverlag AG an der ETH: Zürich and BIOMOS b.v.: Zürich, Groningen, 1996.
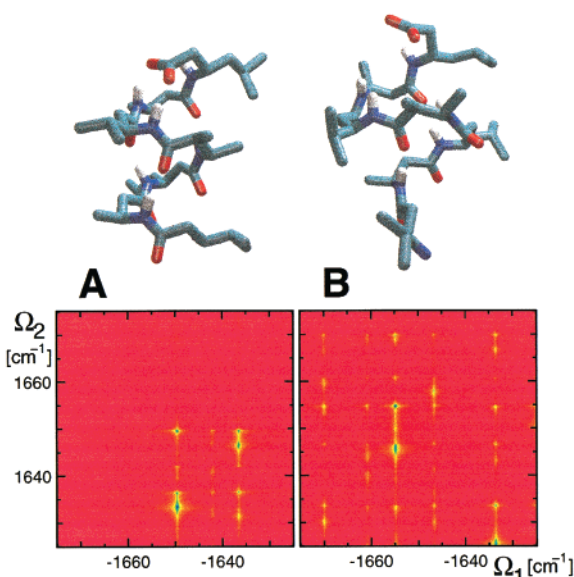

Figure 2. Representative MD structures and single-snapshot vibrational echo spectra for the folded A (NMR structure) and partially unfolded B ensembles. The amide-I chromophores (amide groups with O in red and N in blue) are counted, starting from the N terminus (at the bottom of the structures).

to the solvent and in particular to the modeling of solvent peptide hydrogen bonding. A recent experimental study of an alanine peptide in water[39] found this time scale to be 2 orders of magnitude slower than the simulation. The fast time scale predicted for β-peptides may therefore be changed with an improved modeling of the methanol−peptide couplings.

The solution NMR structure[40] was regenerated in CHARMM from the available NMR data.[40,41] The structure found (structure A in Figure 2) fulfills the NOE and ^3J-coupling constraints. The molecule adopts a left-handed helix (hydrogen bonds between residues i and $i + 2$) consisting of three residues per turn (3_1-helix), in which the amide C=O bonds point in the direction of the N terminus. The rotamers of the side chains were chosen at random. The end groups were protonated (−NH$_3^+$ and −COOH).[41] All β-amino acids were created based on their α-amino equivalents. The topologies and force-field parameters were taken from CHARMM version 27.[42]

A cubic box of 952 explicit methanol solvent molecules was built from a smaller equilibrated box of 119 methanol molecules. The solvent box was centered around the origin, and the center of mass of the peptide was translated to the origin. The peptide was then inserted at the center of the box, and all solvent molecules whose C- or O-atom were within 2.6 Å of any non-hydrogen atom of the peptide were removed. After this procedure the box contained 926 methanol molecules, and the minimal distance of the peptide from the wall of the box was 13 Å. Periodic boundary conditions were applied, and the cutoff range for nonbonded interactions was chosen to be 8−12 Å. To relax the inner shell of methanol molecules surrounding the peptide, the solvent molecules were minimized with all peptide atoms held fixed. A second energy minimization of the entire

(39) Thompson, P. A.; Eaton, W. A.; Hofrichter, J. *Biochemistry* **1997**, *36*, 9200.
(40) Seebach, D.; Ciceri, P. E.; Overhand, M.; Jaun, B.; Rigo, D.; Oberer, L.; Hommel, U.; Amstutz, R.; Widmer, H. *Helv. Chim. Acta* **1996**, *79*, 2043.
(41) Daura, X.; van Gunsteren, W. F.; Rigo, D.; Jaun, B.; Seebach, D. *Chem. Eur. J.* **1997**, *3*, 1410.
(42) MacKerell, A. D., Jr.; Bashford, D.; Bellott, M.; Dunbrack, R. L., Jr.; Evanseck, J. D.; Field, M. J.; Fischer, S.; Gao, J.; Guo, H.; Ha, S.; Joseph-McCarthy, D.; Kuchnir, L. et al. *J. Phys. Chem. B* **1998**, *102*, 3586.

system without constraints was performed to eliminate any residual strain. The SHAKE algorithm[43] was used to constrain the bond lengths to their equilibrium values with a geometric tolerance of 10^{-5}. This allowed us to use a 2 fs integration time step, since it was not necessary to account for bond vibrations. The heating, equilibration, and dynamics runs were performed without any further structural constraints. After minimization and equilibration in CHARMM[42] a 12 ns MD trajectory was generated, and snapshots of the structure were taken every picosecond.

For the first 2 ns the temperature was kept at 300 K where the solution structure is stable, in agreement with the result by Daura et al. which was based on the GROMOS96 force field.[41] To simulate a T-jump, the temperature was raised to 340 K where both structures coexist with equal probability at time 2 ns by scaling the velocities in five steps over a total time of 2 ps. The time-dependent backbone root-mean-square deviation (RMSD) of atom positions in residues 2−6 with respect to the folded NMR solution structure is shown in Figure 1. A RMSD of more than 1 Å (dashed horizontal line) was assumed to be indicative of a partially unfolded structure. The peptide partially unfolds 800 ps after the T-jump, starting from the N terminus, as can be seen from structure **B** in Figure 2. It refolds again and then unfolds more completely.

A set of 3300 structures was taken from the trajectory with a 3 ps time step. This is longer than typical homogeneous dephasing (T_2) and vibrational relaxation times (T_1) that have been experimentally determined to be on the order of ~1 ps for small α-peptides.[32] The snapshots can therefore be considered to be uncorrelated and may be used to model inhomogeneous line-broadening caused by fluctuations in the vibrational frequencies of the chromophores and their couplings. A clustering algorithm described in Appendix A has been used to generate nonoverlapping ensembles of folded and unfolded structures. For a threshold of RMSD ≤ 0.6 Å the algorithm yielded 24 clusters. We have only considered the two largest clusters which contain 1856 unfolded and 1020 folded structures, respectively. The remaining clusters, containing between 1 to ~100 structures, have been discarded.

III. The Fluctuating Vibrational Exciton Model

The application of a vibrational exciton Hamiltonian[14−16] for simulating the amide-I band was proposed in refs 10 and 11. The dipole−dipole coupling of the amide groups undergoes continuous changes due to the protein backbone fluctuations. These fluctuations have been studied by MD simulations,[44] NMR relaxation experiments,[45,46] and by photon echo experiments on spectroscopic probes embedded into the proteins.[47,48] It is necessary to model these changes theoretically in order to extract the related amplitudes and time scales from experiments.[32] Understanding the mechanisms of spectral difusion on the experimental time scale requires a detailed knowledge of the interaction of the chromophores with their environment.

In the following we present a parametrized excitonic model Hamiltonian for the amide-I band that has been generated using a MD trajectory. The heptapeptide is modeled as a system of
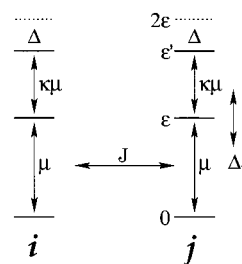
(43) Ryckaert, J. P.; Ciccotti, G.; Berendsen, H. J. C. *J. Comput. Phys.* **1977**, *23*, 327.

(44) Karplus, M.; Petsko, G. A. *Nature* **1990**, *347*, 631.

(45) Bremi, T.; Brüschweiler, R. *J. Am. Chem. Soc.* **1997**, *119*, 6672.

(46) Lienin, S. F.; Bremi, T.; Brutscher, B.; Brüschweiler, R.; Ernst, R. R. *J. Am. Chem. Soc.* **1998**, *120*. 9870.

(47) Joo, T. H.; Jia, Y. W.; Yu, J. Y.; Jonas, D. M.; Fleming, G. R. *J. Phys. Chem.* **1996**, *100*, 2399.

(48) Groot, M.; Yu, J. Y.; Agarwal, R.; Norris, J. R.; Fleming, G. R. *J. Phys. Chem. B* **1998**, *102*, 5923.

Figure 3. The three-level systems representing the peptide plane groups in the exciton Hamiltonian. The levels in each system *i, j* are denoted S_0, S_1, S_2 with energies 0, ϵ, ϵ' and anharmonicity $\Delta = \epsilon' - 2\epsilon < 0$. The levels are shifted by hydrogen bonds to the carbonyl oxygen giving rise to a fluctuating term $\Delta\epsilon$. The only nonvanishing elements of the transition dipole operator are μ and $\mu' = \kappa\mu$, as indicated. The carbonyl vibrations are dipole-coupled where the coupling matrix J_{ij} depends on the local geometries. The couplings between different excited states are given in Appendix B.

$N = 6$ interacting chromophores representing the N peptide bonds. Since we are interested in third-order spectroscopies, we only need to consider the lowest three levels of each peptide group. The i'th peptide is modeled as a three-vibrational-level system denoted $S_0^{(i)}$, $S_1^{(i)}$, $S_2^{(i)}$ with energies 0, ϵ_i, ϵ_i' (see Figure 3). The only nonvanishing elements of the dipole operator correspond to the transitions between $S_0^{(i)} \rightarrow S_1^{(i)}$ and $S_1^{(i)} \rightarrow S_2^{(i)}$ and are denoted μ_i and μ_i', respectively and $\kappa_i \equiv \mu_i'/\mu_i$ is their ratio. For the exciton description of this model we introduce the creation operators $\hat{B}_i^{\dagger}$:[31]

$$\hat{B}_i^{\dagger} = |1\rangle_i\,_i\langle 0| + \kappa_i |2\rangle_i\,_i\langle 1| \qquad (1)$$

The corresponding annihilation operator $\hat{B}_i$ is given by the hermitian conjugate of $\hat{B}_i^{\dagger}$. The polarization operator which describes the coupling to the driving field $-E(t)\hat{P}$ is then given by:

$$\hat{P} = \sum_i \mu_i\,(\hat{B}_i + \hat{B}_i^{\dagger}) \qquad (2)$$

The harmonic part of the Hamiltonian can be represented in the form of coupled harmonic oscillators:

$$\hat{H}_0 = \sum_i \epsilon_i\,\hat{B}_i^{\dagger}\,\hat{B}_i + \sum_{i\neq j} J_{ij}\,\hat{B}_i^{\dagger}\,\hat{B}_j \qquad (3)$$

with transition frequencies ϵ_i and dipole−dipole couplings J_{ij}. The full Hamiltonian (see Appendix B) that describes the optical response of the model contains in addition to $\hat{H}_0$ also an anharmonic term that determines the doubly excited (two-exciton) manifold, the coupling to the laser field, and the coupling to the environment which will be introduced in the next section.

In general, all parameters of this Hamiltonian depend on the peptide conformation and the solvent dynamics and thus fluctuate. In the present study we only included the fluctuations of ϵ_i and J_{ij} which are expected to dominate the spectra. All other parameters were held fixed. The dipole moment ratios κ_i are taken to be time-independent and the same for all chromophores. Setting $\kappa_i = \sqrt{2}$ corresponds to a harmonic mode. The anharmonicities $\Delta = \epsilon_i' - 2\epsilon_i$ (see Figure 3) are also taken to be time-independent and the same for all chromophores. The value of $\Delta = -16$ cm^{-1} is an estimate taken from experiment.[49]

(49) Hamm, P.; Lim, M.; Hochstrasser, R. M. *J. Phys. Chem. B* **1998**, *102*, 6123.
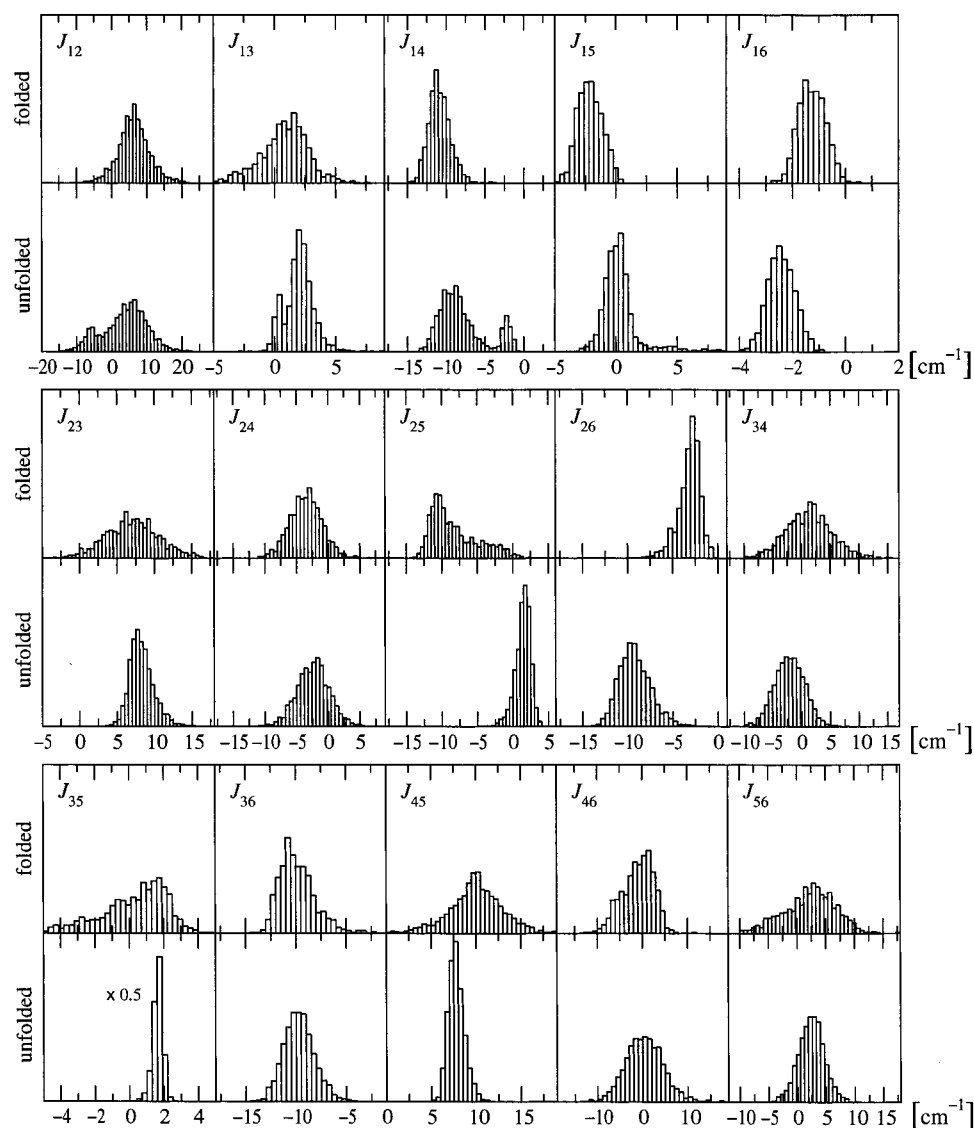
Figure 4. Histograms showing the distribution of the dipolar couplings as fractions of the total number of snaphots in the folded and unfolded clusters, respectively. The ordinate range in all plots is from 0 to 0.25 probability. The histogram for the J_{35} coupling (unfolded) was scaled by a factor of 0.5 to fit in the same range as all other plots. The total distributions of the dipolar couplings as obtained from the 10 ns trajectory (Figure 1) can be generated by adding the folded and unfolded distributions in approximately a 1:2 ratio.

The couplings and transition frequency fluctuations were obtained from the MD simulation of the β-peptide. The excitonic Hamiltonian was constructed for all 2876 peptide conformations contained in the two main MD structure clusters. We have assumed a point dipole coupling among the carbonyl vibrations. The transition dipole–dipole coupling constants (i.e., the off-diagonal elements of the one-exction Hamiltonian) are given by:

$$J_{ij} = \frac{1}{r_{ij}^3}\left(\vec{\mu}_i \cdot \vec{\mu}_j - 3(\vec{n}_{ij} \cdot \vec{\mu}_i)(\vec{n}_{ij} \cdot \vec{\mu}_j)\right) \qquad (4)$$

where $\vec{r}_{ij}$ is the vector connecting the two sites and $\vec{n}_{ij} = \vec{r}_{ij}/r_{ij}$ with $r_{ij} = |\vec{r}_{ij}|$. The magnitude of the transition dipole moments ($|\vec{\mu}_i| = 0.37$ D) and the direction and effective location of the individual point transition dipoles with respect to the peptide group are taken from the model of ref 11. On each CO bond a dipole lying in the peptide plane is placed 0.868 Å away from the carbon atom forming an angle of 25° with the CO bond, pointing toward the nitrogen atom of the peptide bond. Within this point dipole approximation it is straightforward to account

for the statistical distribution of the off-diagonal coupling elements J_{ij} using the conformations from the MD trajectory. The resulting distributions of all 15 coupling constants for the folded and unfolded states are shown in Figure 4.

We have further taken into account fluctuations in the vibrational frequencies ϵ_i induced by hydrogen bonds to N—H groups of other peptide groups within the same molecule. When the oxygen of a particular peptide group is not hydrogen-bonded, the monomeric amide-I frequencies (i.e., the diagonal elements of the one-exction Hamiltonian) are chosen as $\epsilon_i = 1655$ cm^{-1}. It is well-established that hydrogen-bonding causes a red-shift of the monomeric frequency.[50,51] This may be seen, for example, in the difference between the peak position of deuterated *N*-methylacetamide in D$_2$O and in deuterated dimethyl-d_6 sulfoxide, where the latter does not form hydrogen bonds.[49] When the oxygen of a peptide group i is hydrogen-bonded, the monomeric amide-I frequency ϵ_i is red-shifted by a value $\Delta\epsilon_i$ which is linearly dependent on the O$_i$···H distance d_{OH} (given

(50) Krimm, S.; Reisdorf, J. W. C. *Faraday Discuss.* **1994**, *99*, 181.
(51) Torii, H.; Tasumi, T.; Tasumi, M. *Mikrochim. Acta Suppl.* **1997**, *14*, 531.
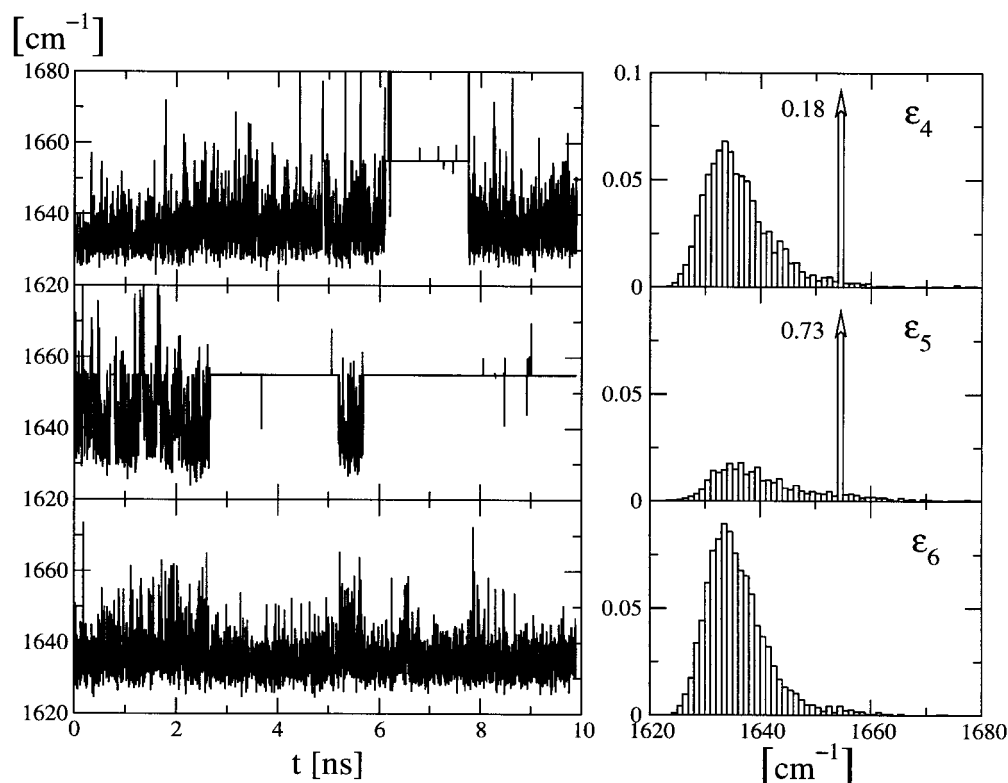
Figure 5. Time dependence of the excitation frequencies ϵ_i of the hydrogen-bonded chromophores $i = 4$, 5, and 6 and the resulting histograms showing the distribution of frequencies as a fraction of the total number of snaphots. The bars at the unshifted (non-hydrogen-bonded) frequency 1655 cm^{-1} are cut off in the histograms of ϵ_4 and ϵ_5. Their actual values are given next to the arrows.

in Å):

$$\Delta\epsilon_i = \alpha_H(2.6 - d_{OH}) \qquad (5)$$

The value of $\alpha_H = -30$ cm^{-1}/Å results in a frequency downshift of ~20 cm^{-1} for a typical hydrogen bond length of 1.9–2.0 Å. A frequency downshift of this order was recently obtained by ab initio calculations[51] but it is smaller than that assumed in ref 50.

The existence of intramolecular hydrogen bonds was determined using the Kabsch−Sander electrostatic energy criterion:[52]

$$E_{KS} = fq_1 q_2 \left(\frac{1}{d_{ON}} + \frac{1}{d_{CH}} + \frac{1}{d_{ON}} + \frac{1}{d_{CH}} \right) \qquad (6)$$

with the constants $q_1 = 0.42$ e, $q_2 = 0.2$ e, $f = 332$ e^{-2} Å kcal/mol, and all distances d measured in Å. The distances are measured between the atoms of the C=O group of one peptide plane and the N−H group of a different peptide plane. A hydrogen bond is deemed to exist if E_{KS} gives a value less than the cutoff −0.5 kcal/mol. A good hydrogen bond (linear, $d_{ON} = 2.9$ Å) has about −3 kcal/mol binding energy. The angle and distance approach is implicitly built into this method. The formula corresponds to a maximum distance of $d_{ON} = 5.2$ Å for in-line atoms and a maximum angle H−N−O of 63°. For each carbonyl group the length of the strongest hydrogen bond was then used to determine the shift $\Delta\epsilon_i$ from eq 5. The resulting trajectory of the transition frequencies of the hydrogen-bonded chromophores is given in Figure 5.

The average values and standard deviations of all vibrational frequencies and couplings obtained by independently averaging the one-exciton Hamiltonians over the ensembles representing the folded and unfolded states are given in Table 1. The total distributions of transition frequencies and couplings can be clearly bimodal (e.g., J_{25}, J_{26}, ϵ_4 in Figures 4 and 5) or strongly non-Gaussian (e.g., J_{15}, J_{35}, ϵ_6). The classification into folded and unfolded structures lifts most of these asymmetries, and the resulting distributions for each structure are mostly Gaussian with the notable exception of parameters involving chromophores at the chain ends. In particular the couplings J_{12} and J_{14} involving the N-terminal chromophore still exhibit a bimodal distribution. This is indicative of the more complete unfolding that takes place in the trajectory around $t = 7.6$ ns.

The average values and variances of the parameters of the Hamiltonian (eq 3) for the folded and unfolded ensembles provide a good measure for the effect of structural fluctuations on the exciton Hamiltonian. We reiterate that the average values and deviations should not be interpreted as parameters for independent Gaussian distributions of diagonal and off-diagonal disorder since the fluctuations in the frequencies and couplings originate from the same changes in the peptide structure and are strongly correlated (see Figure 6).

The average frequencies $\bar{\epsilon}_i$ of the hydrogen-bonded chromophores 4, 5, and 6 of the folded peptide are red-shifted by about 20 cm^{-1}. This can be seen by comparing Table 1 with the three-dimensional structure in Figure 2, in which the hydrogen bonds between peptide planes i and $(i + 3)$ are visible. It also applies to chromophore 6 and mostly to chromophore 4 of the unfolded structure, while chromophore 5 is not hydrogen-bonded in the unfolded state (see the trajectories in Figures 5 and 6). The average fluctuation of the transition frequency due to hydrogen bonds is 5–10 cm^{-1} for hydrogen-bonded residues. Average couplings between different chromophores are typically in the range of −10–10 cm^{-1} with standard deviations of σ_{ij} < 4.5 cm^{-1} for the folded ensemble and σ_{ij} < 6.4 cm^{-1} for the unfolded set. The couplings show a typical pattern due to the

(52) Kabsch, W.; Sander, C. *Biopolymers* **1983**, *22*, 2577.

J. Am. Chem. Soc., Vol. 123, No. 13, 2001

Scheurer et al.

Table 1. Average Values $\bar{\epsilon}_i$ and Standard Deviations σ_i of the Diagonal Elements of the Fluctuating One-Exciton Hamiltonian (See Eq 3) and Average Couplings $\bar{J}_{ij}$ and Their Standard Deviations σ_{ij} for the Folded and Unfolded State

	Folded					
i	1	2	3	4	5	6
$\bar{\epsilon}_i$	1655.00	1655.00	1655.01	1635.09	1643.38	1637.59
σ_i	0.00	0.00	0.31	5.94	10.61	6.63
j		$\bar{J}_{ij}$				
1		6.41	0.80	−10.83	−2.10	−1.25
2			7.12	−3.49	−8.20	−3.12
3				1.35	0.23	−9.84
4					9.95	−0.96
5						2.24
j		σ_{ij}				
1		4.47	1.98	1.39	1.00	0.50
2			3.51	2.54	3.34	1.21
3				4.03	1.99	1.80
4					3.07	3.41
5						4.52
	Unfolded					
i	1	2	3	4	5	6
$\bar{\epsilon}_i$	1655.00	1655.00	1655.00	1640.06	1655.00	1634.93
σ_i	0.00	0.00	0.00	9.18	0.10	4.46
j		$\bar{J}_{ij}$				
1		3.62	1.99	−7.99	0.42	−2.42
2			8.30	−2.41	1.39	−9.20
3				−2.12	1.62	−9.73
4					7.78	0.39
5						2.40
j		σ_{ij}				
1		6.32	1.16	3.01	1.96	0.51
2			1.61	2.61	1.09	1.75
3				2.64	0.29	1.50
4					0.90	4.13
5						2.25
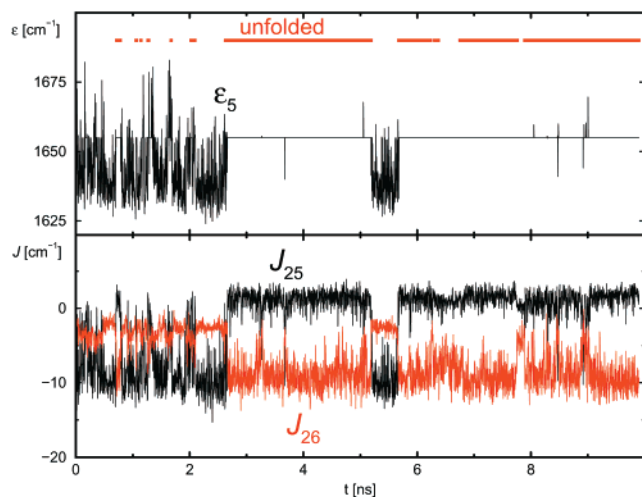
Figure 6. Time dependence of the excitation frequency ϵ_5 and the couplings J_{25} and J_{26}. The strong geometric correlation between different parameters of the Hamiltonian is clearly visible. The broken line in the upper plot represents the snapshots that belong to the unfolded ensemble.

helical structure of the peptide in the folded state with a large negative value of approximately −9 cm^{-1} for the coupling between peptide planes i and $(i + 3)$. This changes during
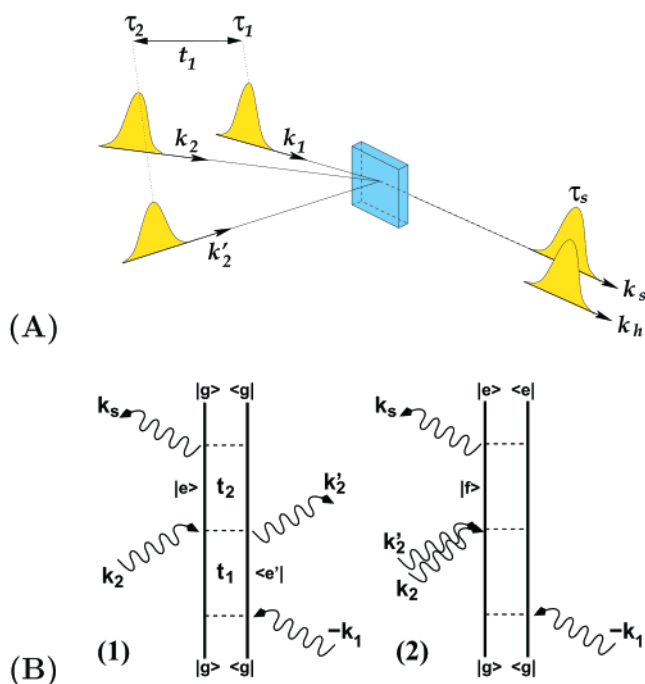
Figure 7. (A) Pulse configuration and timing of the three-pulse photon echo experiment. The first pulse ($\mathbf{k}_1$) is at time τ_1 followed by a pulse pair ($\mathbf{k}_2,\mathbf{k}'_2$) at time τ_2. The echo signal at $\mathbf{k}_s = \mathbf{k}'_2 +\mathbf{k}_2 − \mathbf{k}_1$ is detected by mixing it with an additional heterodyne pulse k_h at time τ_s. The time variables of the two-dimensional experiment are $t_1 = \tau_2 − \tau_1$ and $t_2 = \tau_s − \tau_2$. (B) Two-sided Feynman diagrams representing the $|S^{(1)}|$ (left diagram) and the $|S^{(2)}|$ component (right diagram) of the vibrational echo signal. The relevant states are labeled $|g\rangle$ for the ground state, $|e\rangle$ and $|e'\rangle$ for different first excited states and $|f\rangle$ for the two exciton state (see appendix B). t_1,t_2 are the time delays between the pulses.

unfolding where the (1, 4) and (3, 6) couplings persist, while the (2, 5) coupling is replaced by (2, 6), as is evident from Figures 4 and 6. This yields a strongly coupled subsystem of chromophores 2, 3, and 6 giving rise to cross-peaks in the 2D vibrational echo spectrum. The loss of the typical helical coupling pattern induces clearly observable changes in the 2D spectra as will be shown next.

IV. 2D Vibrational Echo Spectra

The lowest-order nonlinear-IR spectroscopy in non-centrosymmetric media requires three pulses. In the photon echo technique (see Figure 7) two of the three pulses are time-coincident and only differ by their wave vector. The system thus interacts with a single pulse with wave vector $\mathbf{k}_1$ at time τ_1 and twice with the pulse pair ($\mathbf{k}_2$ $\mathbf{k}'_2$) at time τ_2. The delay between the single pulse and the pulse pair will be denoted $t_1 = \tau_2 − \tau_1$. The resulting echo signal in the direction $\mathbf{k}_s = \mathbf{k}'_2 + \mathbf{k}_2 − \mathbf{k}_1$[21,53,54] is detected by mixing with an additional heterodyne pulse $\mathbf{k}_h$ at time τ_s. This gives the second time variable $t_2 = \tau_s − \tau_2$ of the 2D experiment. Heterodyne (time-gated) detection yields the time-resolved signal $S(t_2, t_1)$, maintaining the information about its phase, that is, its real and imaginary parts. In the following we assume that all three incident pulses as well as the heterodyne pulse are linearly and parallely polarized.

Closed expressions for the third-order nonlinear response function which determines all 2 and 3 D spectroscopies for this

(53) Chernyak, V.; Wang, N.; Mukamel, S. *Phys. Rep.* **1995**, *263*, 213.
(54) Zhang, W. M.; Chernyak, V.; Mukamel, S. *J. Chem. Phys.* **1999**, *110*, 5011.

model were derived in ref 31 by solving the NEE for the exciton Hamiltonian introduced in section III. We assume that the coupling to other vibrations and solvent modes conserves the number of excitons and its effects are incorporated through the dephasing rates of the single exciton and the two-exciton transitions. In all our simulations we have taken them to be Γ and 2Γ respectively. The corresponding expressions for the 2D signals in the frequency domain were obtained in ref 54 by a double Fourier transformation of the time domain signal:

$$S(\Omega_2,\Omega_1) = \int_0^\infty dt_2 \int_0^\infty dt_1 \exp(i\,(\Omega_1 t_1 + \Omega_3 t_2))S(t_2, t_1) \quad (7)$$

This form is particularly useful for displaying structural information in terms of cross-peaks, in analogy with 2D NMR. In our simulations we have used the closed expressions for the calculation of the 2D vibrational echo signals given in Appendix E of ref 54. The total 2D signal is decomposed into two contributions (eqs E1 and E2 of ref 54). The first component $S^{(1)}(\Omega_2\ \Omega_1)$ represents correlations between one-exciton states described by the Feynman diagram (1) in Figure 7. The second component $S^{(2)}(\Omega_2\ \Omega_1)$ is due to correlations between the one- and two-exciton manifolds and is represented by the Feynman diagram (2) in Figure 7. The individual components $S^{(1)}$ and $S^{(2)}$ are not observable but are a useful theoretical decomposition of the total signal that helps tracing the origin of specific features of the 2D spectra.

The 2D vibrational echo spectra were calculated for different values of the dephasing rate Γ. Two typical single-snapshot spectra are shown in Figure 2 where an artificially small value of 0.2 cm^{-1} was chosen for the homogeneous line-broadening parameter Γ in order to resolve all diagonal and cross-peaks. The analysis of these single-structure spectra can be performed in analogy to that of the glycine dipeptide discussed in ref 20. In the spectrum for the folded structure **A** two distinct diagonal peaks are visible. The 1650 cm^{-1} peak can be attributed to the chromophores 1−3 (counted from the N terminus of the peptide) which are not hydrogen-bonded, as can be seen in the structure displayed above the 2D spectrum. The 1637 cm^{-1} peak belongs to the strongly hydrogen-bonded chromophores 4−6. These are involved in the core of the 3_1 helix. The strong $(i, i + 3)$ coupling (see Table 1) gives rise to the cross-peaks between the two diagonal peaks. The asymmetry is a result of the two-exciton dynamics that only takes place after the first pulse and that is governed by the anharmonic part of the total exciton Hamiltonian. The spectrum of the unfolded structure **B** still contains the two distinct diagonal peaks for the hydrogen-bonded and the free chromophores. Yet the more complicated and geometrically less well-defined structure yields a larger number of weak cross-peaks that reveal the rich coupling pattern of the six chromophores. The asymmetry due to anharmonicity affecting the two-exciton dynamics is again clearly visible and gives rise to strong peaks that are displaced by approximately −10 cm^{-1} from the diagonal in the direction of Ω_2. This anharmonic shift, which is smaller (in absolute magnitude) than the anharmonicity Δ of the localized vibrations, indicates that the observed peaks are of excitonic and not of localized nature.

The spectra of the unfolded and the folded set were then averaged separately to account for structural fluctuations. The resulting inhomogeneously broadened spectra for the folded (unfolded) state are shown in Figure 8 top (bottom). The left column in each panel displays the linear absorption for four different values of the homogeneous broadening parameter $\Gamma = 0.2, 1, 5, 10$ cm^{-1}. The experimental homogeneous broadening in similar systems corresponds to a value of $\Gamma \approx 5-10$

cm^{-1}.[32] The linear absorption of the folded peptide consists of a broad peak with maximum intensity at 1640 cm^{-1} that is due to the hydrogen-bonded chromophores, and a small blue-shifted shoulder caused by the free carbonyl groups. Unfolding yields a second 1655 cm^{-1} peak due to the loss of hydrogen-bonded helical structure of the peptide. This is in agreement with experimental linear absorption studies of T-jump induced unfolding processes in natural helical α-peptides.[17]

The effects of realistic fluctuations of the excitonic Hamiltonian that are due to structural changes of the peptide are most easily visible if the single-structure spectra in Figure 2 are compared to the corresponding ensemble-averaged spectra with the same choice of a small value of 0.2 cm^{-1} for the homogeneous broadening parameter Γ. These spectra are displayed in the top rows of both panels of Figure 8.

The total signal ($|S(\Omega_1, \Omega_2)|$) for the folded structure consists of one inhomogeneously broadened peak stretched along the diagonal ($\Omega_1 = -\Omega_2$) with a maximum centered around 1640 cm^{-1}. The maximum is asymmetric and inhomogeneously broadened along the anti-diagonal of the spectrum. It corresponds to the strongly hydrogen-bonded and thus red-shifted CO groups in the peptide planes 4−6. The broadening along the diagonal is mainly caused by changes in the vibrational frequencies due to hydrogen bond fluctuations. The free chromophores peak is weak and overlaps with the diagonal signal trace from the hydrogen-bonded sites. No cross-peaks are visible after the averaging since the typical fluctuations (Table 1) of the coupling elements are considerably larger than the homogeneous line width.

This also applies to the real and imaginary part of the signal (which may be observed separately using heterodyne detection), given in the third column labeled $\mathcal{R}S(\Omega_1, \Omega_2)$ and the fourth column labeled $\mathcal{T}S(\Omega_1, \Omega_2)$, respectively. The real component exhibits the same features as the total signal and the antisymmetric peak due to the anharmonicity of the system is resolved. The imaginary part is less broadened than the total signal due to its dispersive nature. As expected, the vibrational echo technique refocuses the inhomogeneous broadening of the one-exciton dynamics. This is clearly visible in the $|S^{(1)}|$-component which depends on the one-exciton dynamics only. The broadening of this component which is visible for very small homogeneous line width is due to unresolved couplings between the chromophores. The $|S^{(2)}|$-component cannot be completely refocused in the echo experiment since it depends on the coupling between one- and two-exciton dynamics. This component is additionally broadened by the anharmonic contribution which gives rise to a signal parallel to the main peak and displaced from it by approximately −10 cm^{-1} in the Ω_2-direction. It is this contribution to $|S^{(2)}|$ which renders the total signal nonsymmetric in Ω_1 and Ω_2 due to the fact that two-exciton dynamics can only occur during the t_2 period after the initial pulse. It is clear that the peaks in the spectrum are of excitonic nature since the anharmonic shift is again smaller than Δ. The calculation of one- and two-exciton energies for the average Hamiltonians in Table 1 gives a range of 1625−1671 cm^{-1} for the one-exciton energies in the folded state and 3250−3350 cm^{-1} for the two-exciton energies in the folded state (see Table 2). The anharmonic shift is therefore compatible with the excitonic structure of the system (see Appendix B).

The analysis of the top row of spectra in Figure 8 for the unfolded peptide is similar to the folded case. The total signal $|S(\Omega_1, \Omega_2)|$ shows that the unfolding leads to the appearance of a group of peaks around 1660 cm^{-1} and above, which corresponds to free CO groups. These peaks are now well-
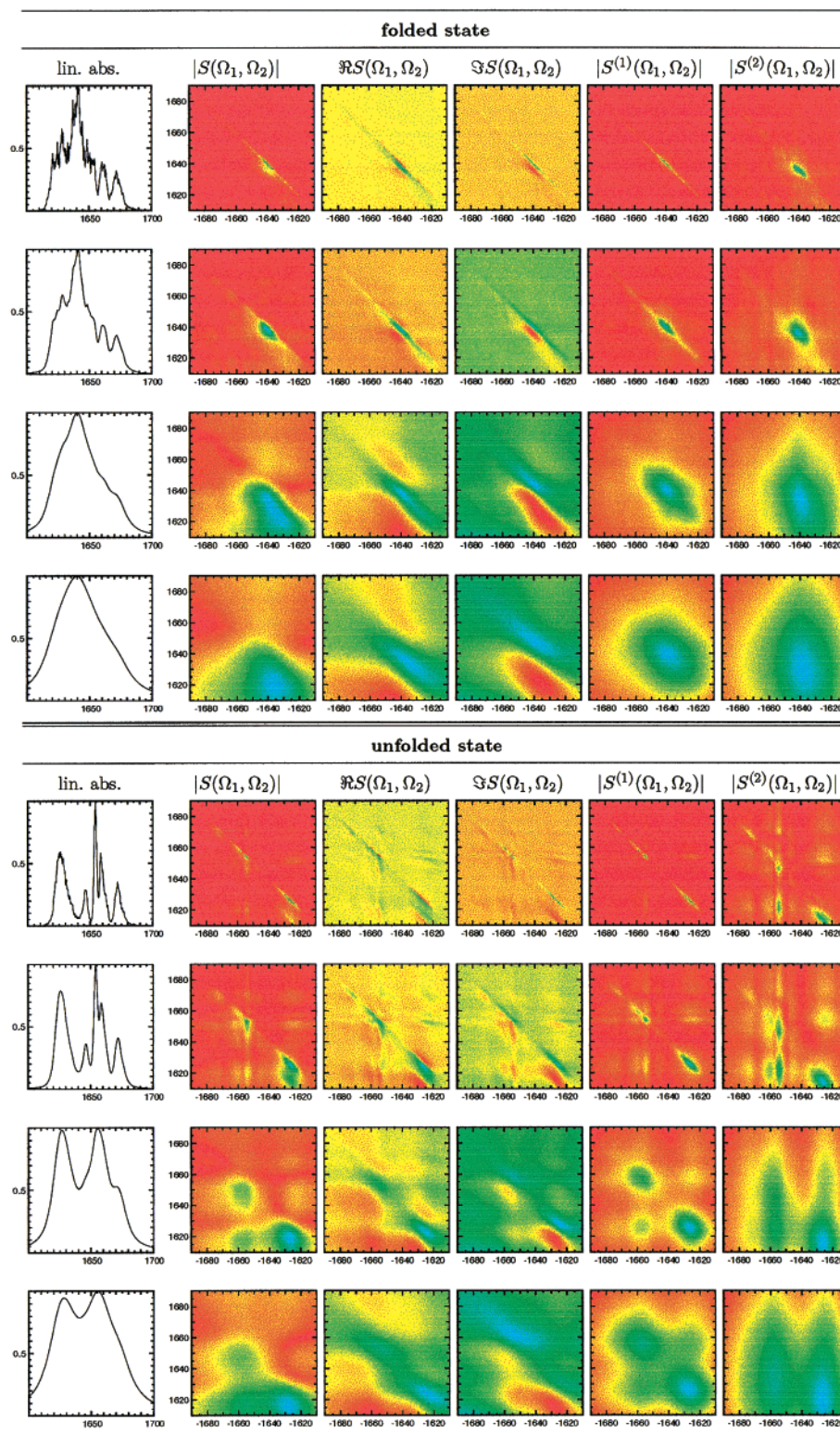
Figure 8. Averaged vibrational echo spectra for the folded and unfolded state. The signal intensities are given in arbitrary units, frequencies are in cm^{-1}. The 2D spectra are displayed with Ω_1 on the abscissa and Ω_2 on the ordinate. The four rows differ by the value of the homogeneous line width parameter Γ which is from the top: $\Gamma = 0.2, 1, 5, 10$ cm^{-1}. The left column gives the linear absorption. The following columns show successively the absolute value of the total signal, its real part, its imaginary part, the one-exciton contribution, and the two-exciton contribution, as indicated. The individual components $|S^{(1)}|$ and $|S^{(2)}|$ are not observable but are a useful theoretical decomposition of the total signal that helps analyzing specific features of the 2D spectra (see ref 54).

resolved, and cross-peaks with the hydrogen-bonded groups are visible even for the extremely small homogeneous line width chosen in the first row of spectra. Most of the cross-peaks that are resolved in the single-structure spectrum of Figure 2B are not visible in the averaged spectrum. As for the folded case

this is due to the extremely small homogeneous line width in comparison to the typical fluctuations in the couplings between the chromophores. The weak cross-peaks from several different single-structure spectra typically do not overlap since they are very narrow and well separated in the 2D spectrum due to the

Table 2. One- and Two-Exciton Energies Obtained as Eigenvalues of the Average Hamiltonians Given in Table 1 for the Folded and Unfolded State

Folded					
one-exciton energies $\bar{\epsilon}_i$					
1625.50	1633.24	1641.73	1649.09	1659.98	1671.51
two-exciton energies $\bar{\epsilon}_i$					
3249.51	3260.97	3269.87	3270.50	3281.48	3284.76
3288.00	3291.04	3297.18	3297.46	3301.00	3304.01
3306.70	3310.94	3315.27	3317.16	3319.49	3326.45
3328.82	3338.72	3349.89			
Unfolded					
one-exciton energies $\bar{\epsilon}_i$					
1628.63	1634.68	1646.57	1654.30	1659.77	1671.02
two-exciton energies $\bar{\epsilon}_i$					
3261.59	3263.75	3272.97	3285.13	3288.04	3292.74
3293.55	3295.99	3299.11	3302.01	3302.19	3308.71
3310.74	3310.88	3314.94	3318.47	3321.87	3322.18
3329.87	3336.70	3348.68			

coupling fluctuations. Taking the average over a large number of spectra then reduces dramatically the intensities of all cross-peaks (i, j) with coupling fluctuations $\sigma_{ij} \gg \Gamma$ (see Table 1). A few additional weak cross-peaks are visible in the real part since it is slightly more broadened. The imaginary part of the spectrum is less broadened and shows well-resolved anharmonic peaks displaced parallel to the diagonal. The one-exciton component $|S^{(1)}|$ is completely refocused and symmetric while $|S^{(2)}|$ exhibits a strong asymmetry and large inhomogeneous broadening in the Ω_2 direction that is not refocused in the echo experiment.

The second rows of spectra in both panels of Figure 8 are simulated with a homogeneous line width of $\Gamma = 1$ cm^{-1}. This value is still small compared to the experiment, but it provides a good compromise between homogeneous broadening and inhomogeneous averaging effects that allows to see more clearly the spectral features discussed for the first row. The spectra are still as well resolved as for $\Gamma = 0.2$ cm^{-1} but with a larger line width that is on the order of the coupling fluctuations (σ_{ij} in Table 1), the cross-peaks do not disappear upon averaging. This is clearly visible in the case of the total signal and the one-exciton component of the unfolded state which shows a set of well-resolved cross-peaks between the free and the hydrogen-bonded chromophores.

The experimental value of the homogeneous line width for small helical α-peptides is on the order of 5−10 cm^{-1}.[32] The last two rows in both panels of Figure 8 show spectra with $\Gamma = 5$ and 10 cm^{-1}, respectively. Preliminary experiments[55] suggest that the homogeneous broadening for a related β-peptide is in this range. The 2D vibrational echo exhibits a higher resolution compared to the linear absorption signal even for large homogeneous broadening. The broadened peaks are more clearly resolved in the 2D spectrum, especially if the real and imaginary parts of the spectrum are taken into account. The existence of cross-peaks allows one to decide whether a strongly broadened diagonal peak consists of two coupled individual signals or a single resonance.

The 2D vibrational echo signals carry a much higher information content than 1D techniques (linear absorption). The cross-peaks also contain information about the molecular geometry since the coupling strength depends on the relative orientation of the transition dipoles. Nonlinear spectroscopy additionally provides information about anharmonicities and overtones which often have low intensity in linear absorption spectra due to the small transition dipole moments for the direct

$S^{(0)} \rightarrow S^{(2)}$ transition. A generalization of the experiment presented in this paper, which can also be described by the present fluctuating exciton Hamiltonian, is the three-pulse echo where a variable delay T is used between the second and third pulse. This experiment has been discussed for dimers, and new peaks have been predicted.[56−58] The variation of the delay T allows one to measure the time scales of vibration relaxation processes directly. Additional information is obtained from the phase of the signal by deploying its spectrogram (time- and frequency-gated signal).[59,60] Photon echo spectroscopy refocuses the inhomogeneous broadening of the one-exciton evolution and therefore makes it possible to discriminate between homogeneous and inhomogeneous broadening contributions. Other spectroscopic techniques will have to be developed that can also overcome homogeneous broadening, making use of ultrafast detection and coherence manipulation. These techniques could strongly enhance the resolution achieved by vibrational spectroscopy of complex systems.

V. Conclusions

By combining MD simulation, a fluctuating exciton Hamiltonian for the amide-I band, and the NEE approach for the calculation of 2D vibrational spectra we have computed 2D vibrational echo signals with realistic structural fluctuations beyond simple uncorrelated stochastic disorder. The advantage of the NEE over a conventional sum over states calculation lies in its more favorable scaling with the number of chromophores N. The most demanding task in modeling the two-exciton dynamics, the calculation of the exciton scattering matrix $\bar{\Gamma}$,[31,54] scales as N^2 which renders the total 2D signal calculation a task of order $\sim N^4$. This is in contrast to a sum over states calculation which requires the diagonalization of the two-exciton Hamiltonian, which scales as N^4, thus making the signal computation scale as $\sim N^6$. This gain in computational efficiency allows us to perform a large number of calculations based on the geometries taken from an MD trajectory to account for structural fluctuations by ensemble averaging over the MD snapshots. The approach was applied to the unfolding dynamics of a helical β-heptapeptide following a T-jump. The resulting linear absorption spectra closely resemble experimental results for helical α-peptides for a reasonable choice of homogeneous broadening. The 2D spectra contain additional geometric information in the form of cross-peaks between hydrogen-bonded and free carbonyl groups in case of the unfolded state. The asymmetry of the spectra in the folded as well as the unfolded state carries information about the two-exciton dynamics and therefore about the anharmonicities of the amide-I vibrations. The simulated spectra show that 2D vibrational echo spectroscopy can probe the fast structural changes during unfolding following a T-jump more easily than linear absorption spectroscopy. This should make the measurement of the time scales involved in the unfolding process more reliable. Reversible unfolding and folding in an MD simulation has been achieved for a three-stranded synthetic β-sheet peptide,[61] which would be an interesting candidate to study with the present approach.

(56) Piryatinski, A.; Chernyak, V.; Mukamel, S. *Chem. Phys.* **2001**. In press.
(57) Asplund, M. C.; Zanni, M. T.; Hochstrasser, R. M. *Proc. Natl. Acad. Sci. U.S.A.* **2000**, *97*, 8219.
(58) Zhang, W. M.; Meier, T.; Chernyak, V.; Mukamel, S. *J. Chem. Phys.* **1998**, *108*, 7763.
(59) Meier, T.; Chernyak, V.; Mukamel, S. *J. Chem. Phys.* **1997**, *107*, 8759.
(60) Mukamel, S. *J. Chem. Phys.* **1997**, *107*, 4165.
(61) Ferrara, P.; Caflisch, A. *Proc. Natl. Acad. Sci. U.S.A.* **2000**, *97*, 10780.

(55) Hamm, P. Private communication.

The present Hamiltonian is based on several approximations. First, the only term in the Hamiltonian that includes the effects of the peptide geometry on the frequencies ϵ_i is the hydrogen bonding. Fluctuations of the vibrational frequencies caused by local deformations of the peptide plane or by hydrogen bonding to solvent molecules are neglected. Our present simulations thus underestimate the effect of the local peptide plane geometry on the spectra. In particular the differences between the vibrational frequencies of different peptide planes that are due to the side chain pattern of the peptide are neglected. These approximations especially affect the inhomogeneous broadening of the unfolding peaks which is underestimated in the current calculations since it is solely caused by unresolved couplings. The substructure of the unbonded peaks for small homogeneous line width may be more difficult to resolve with a more realistic Hamiltonian that also includes hydrogen-bonding effects to the solvent and changes in the transition frequency due to local geometric fluctuations.

Whether the dipole approximation for the off-diagonal coupling elements is adequate for a quantitative description of all spectroscopic features needs to be tested. These approximations may be relaxed by direct quantum chemical calculations for all parameters of the vibrational exciton Hamiltonian for each individual MD structure. This will also include couplings due to nonlocal anharmonicities of the molecular potential energy surface. Very little is known about the effects of these contributions on multidimensional peptide spectra. A thorough future examination of these effects is important for the interpretation of experimental spectra.

Multidimensional IR spectroscopy has become an important tool for studying fast protein folding and unfolding dynamics. It is therefore necessary to classify the possible spectroscopic techniques according to their information content and evaluate their potential use for studying protein dynamics. The 2D spectra presented here with realistic line-broadening parameters show distinct signatures of the folded and unfolded states and allow to follow the motions on the folding time scale. More elaborate pulse sequences, the use of phase-locked pulses, and selective isotopic substitution (N(15), C(13)) of peptide bonds may provide much more detail and allow targeted assignments of specific spectral features which are not possible using 1D techniques. The calculation of the full third-order response based on our microscopic model should allow us to simulate all possible three-pulse experiments including relaxation and exciton transport effects through the Redfield formalism. This should allow devising three-dimensional experiments that will yield all accessible information about the third-order response which might not be easily extracted from a single 2D experiment due to limited resolution and line-broadening effects.

Appendix A: The Clustering Algorithm

We have used a clustering algorithm for classifying structures generated by the MD simulations as folded and unfolded. It consists of the following steps:

1. Choose a cut-off distance d.

2. Initialize the list of remaining structures l to contain all structures.

3. For each entry in l, determine all structures contained in l that are within a backbone (residues 2−6) RMSD distance from it that is lower than the threshold d. These make up the entries neighbor list.

4. Pick the entry from l with the largest number of neighbors. This entry is a new cluster center.

5. Assign all neighbors of the cluster center to this cluster and remove them from the list of remaining structures l.

6. Repeat the steps starting from 3 until no structure remains in l.

This procedure yields a set of distinct (mutually nonoverlapping) clusters.

Appendix B: The Vibrational Exciton Hamiltonian

The full Hamiltonian that describes the optical response of the system is:[31,54]

$$\hat{H} = \hat{H}_0 + \sum_j \frac{g_j}{2}(\hat{B}_j^\dagger)^2 (\hat{B}_j)^2 + \hat{H}_{\text{phonon}} - \mathcal{E}(t)\hat{P} \quad \text{(B1)}$$

where $\hat{H}_0$ is given in eq 3 and $g_j = 2(\epsilon_j'\kappa_j^{-2} - \epsilon_j)$ is an anharmonicity parameter.

The one-exciton manifold is determined by the energies and dipole−dipole couplings J_{ij}. The two-exciton manifold is determined by the anharmonicities $\Delta_i = \epsilon_j' - 2\epsilon_i$ and the dipole moment ratios κ_i. The bath Hamiltonian $\hat{H}_{\text{phonon}}$ and its coupling to the chromophores is assumed to conserve the number of excitons, and its effects are incorporated through the dephasing rate Γ.

The one-exciton states and energies can be readily obtained by diagonalization of the matrix representing the one-exciton Hamiltonian $h_{ij} = \delta_{ij}\epsilon_i + J_{ij}$. The two-exciton manifold is obtained from the representation of the Hamiltonian $\hat{H}$ in the basis of all possible double excitations and is denoted $h^{(2)}$, which is a Hermitian matrix. The double excitations can be separated into two distinct classes, overtone excitations (OTE) $\hat{B}_i^\dagger \hat{B}_i^\dagger |0\rangle$ and collective excitations (CTE) $\hat{B}_k^\dagger \hat{B}_j^\dagger |0\rangle$ ($i \neq j$), where $|0\rangle$ denotes the global ground (vacuum) state of the system. For N chromophores there are N OTE and $N(N - 1)/2$ CTE states yielding a total of $N(N + 1)$ double excited states.

The only nonzero matrix elements of $h^{(2)}$ between doubly excited states $\hat{B}_k^\dagger \hat{B}_l^\dagger |0\rangle$ and $\hat{B}_k^\dagger \hat{B}_j^\dagger |0\rangle$ ($i, j, k, l = 1, ..., N$) are given by:

$$\kappa_i^2 \left(\epsilon_i + \frac{g_i}{2}\right) \quad \text{if} \quad i = j = k = l \quad \text{(B2)}$$

$$\kappa_i J_{ik} \quad \text{if} \quad i = j = l \neq k \quad \text{(B3)}$$

$$\epsilon_i + \epsilon_j \quad \text{if} \quad i = k \neq j = l \quad \text{(B4)}$$

$$J_{ik} \quad \text{if} \quad i \neq j = l \neq k \quad \text{and} \quad i \neq k \quad \text{(B5)}$$

Using the average values of the one-exciton Hamiltonian matrix elements h_{ij} for the folded and unfolded state given in Table 1, we obtain the one-exciton and two-exciton energies given in Table 2. The possible cross-peak positions ($-\epsilon_i$, $\epsilon_j' - \epsilon_i$) of peaks due to the Feynman diagram (2) in Figure 7B are given by all combinations of one-exciton energies ϵ_i ($i = 1, ..., N$) and two-exciton energies ϵ_j' ($j = 1, ..., N(N +1)/2$). These positions may be compared to the averaged spectra. Yet, due to the nonlinearity of the spectroscopy, the spectra calculated from average Hamiltonians will not be the same as the average over the ensemble of spectra. This reflects the extra information obtained from multidimensional techniques.